Wind and Structures, Vol. 16, No. 2 (2013) 193-211
DOI: http://dx.doi.org/10.12989/was.2013.16.2.193

Laboratory measurements of the drag coefficient over a fixed shoaling hurricane wave train

Brian C. Zachry[*1,2], Chris W. Letchford[3], Delong Zuo[1] and Andrew B. Kennedy[4]

[1]*Wind Science and Engineering Research Center, Texas Tech University, Lubbock, TX 79409, USA*
[2]*AIR Worldwide, Boston, MA 02116, USA*
[3]*Department of Civil and Environmental Engineering, Rensselaer Polytechnic Institute, Troy, NY 12180, USA*
[4]*Department of Civil Engineering and Geological Sciences, University of Notre Dame, Notre Dame, IN 46556, USA*

(Received June 8, 2011, Revised December 14, 2011, Accepted January 30, 2012)

Abstract. This paper presents results from a wind tunnel study that examined the drag coefficient and wind flow over an asymmetric wave train immersed in turbulent boundary layer flow. The modeled wavy surface consisted of eight replicas of a statistically-valid hurricane-generated wave, located near the coast in the shoaling wave region. For an aerodynamically rough model surface, the air flow remained attached and a pronounced speed-up region was evident over the wave crest. A wavelength-averaged drag coefficient was determined using the wind profile method, common to both field and laboratory settings. It was found that the drag coefficient was approximately 50% higher than values obtained in deep water hurricane conditions. This study suggests that nearshore wave drag is markedly higher than over deep water waves of similar size, and provides the groundwork for assessing the impact of nearshore wave conditions on storm surge modeling and coastal wind engineering.

Keywords: drag coefficient; shoaling wave; wind stress; profile method; log-law

1. Introduction

Momentum exchange at the air-sea interface, described by a drag coefficient C_D, based on wind speed at 10 m, has been studied extensively since the pioneering work of Charnock (1955), and recently received increased attention at the turn of the century. This is primarily due to the initiative to provide better wave, current, and surge forecasts in hurricane conditions. A comprehensive understanding of momentum exchange in the shoaling wave region is critical for the accurate prediction of storm surge. Here, nearshore wind stresses generate wind setup, which is a rise in the mean water level (MWL) at the downwind coast. This phenomenon is particularly important in coastal areas with wide and shallow continental shelves, as wind setup is inversely proportional to water depth and hence the primary contributor to the overall surge in shallow water. With all else being constant, it is the underlying roughness elements (i.e., the shape, height, and frequency of waves) that govern the magnitude of wind setup.

∗Corresponding author, Dr., E-mail: Brian.Zachry@noaa.gov

It is well known that wave interaction with the local bathymetry causes wave conditions in shallow water to be markedly different from those in deep water. The nearshore region is characterized by a rapidly evolving water surface profile due to wave shoaling and breaking transformation processes. According to wave theory, shoaling waves increase in height and steepness, become increasingly asymmetric, and essentially rougher in an aerodynamic sense with shoreward progression (i.e., as the waves propagate towards the shore and prior to the onset of wave breaking) than their deep water sinusoidal counterparts. Since the majority of wind setup occurs in the shoaling region compared to offshore, it is hypothesized that the nearshore wind stress is significantly larger than that over deep water due to the facts that nearshore waves: (1) have steep and nonlinear profiles, (2) propagate more slowly as they interact with the sea bed, (3) have rapidly varying surface wave fields, and (4) can be significantly misaligned with the mean wind. Based on these differences, separate drag coefficient parameterizations for nearshore and offshore wave regions are likely necessary to accurately quantify air-sea momentum exchange and thus estimate surge at the coast.

At present, nearshore wind stress is not completely known and only a few studies exist on this topic. Consequently, deep water surface drag coefficient parameterizations are commonly used for storm surge modeling and analysis (e.g., Westerink *et al.* 2008). Anctil and Donelan (1996) observed higher drag over shoaling waves compared to both deep water and breaking waves in Lake Ontario, Canada. For wind speeds of around 14 ms^{-1}, they estimated the shoaling wave drag coefficient to be 0.0028, which is roughly 40% higher than deep water values at similar wind speeds (e.g., Powell *et al.* 2003, Donelan *et al.* 2004, Black *et al.* 2007, Jarosz *et al.* 2007). Data reported in Powell (2008) also suggest increased drag in the nearshore region. Based on these studies and the differences stated above, deep water wind stress parameterizations do not allow for reliable estimation of the nearshore wind setup and are a potential culprit for the under-prediction of surge. In addition, the many deep water formulations that exist can result in large differences in predicted surge heights (e.g., Weaver 2004). Unfortunately, engineers currently lack the quality datasets required to fully understand this phenomenon, as it is extremely difficult to obtain collocated wind and wave measurements in the coastal region. Hence, laboratory simulation becomes vital to expanding our knowledge of nearshore wind stress.

Accurate simulation of nearshore water waves in the laboratory is extremely challenging and often impractical. As a result, fixed wave models are often utilized to address key aspects of the flow physics (e.g., Belcher and Hunt 1998). This methodology is considered acceptable, but there are fundamental aerodynamic differences between air flow over natural water waves and stationary rigid models, which includes but is not limited to the surface boundary conditions, the free surface mobility, and the onset of flow separation. For the latter, rigid waves in the wind tunnel tend to be more prone to separation than actual water waves (e.g., Banner and Melville 1976, Csanady 2001). Despite these differences, numerous laboratory experiments have studied air flow over sinusoidal wave trains and have provided valuable results (e.g., Zilker and Hanratty 1979, Buckles *et al.* 1984, Kuzan *et al.* 1989, Belcher and Hunt 1998, Gong *et al.* 1999). Most authors were interested in studying the spatial variation of the flow field, shear stress, and pressure along the wave surface to develop a better understanding of wind wave generation and surface currents. The latter is measured in terms of a form drag on the wave surface (e.g., Stanton *et al.* 1932). A wide variety of wave steepness has been studied, ranging from very steep H/L = 0.4 (e.g., Beebe 1972), to steep H/L = 0.2 (e.g., Buckles *et al.* 1984, Gong *et al.* 1999), to gentle-sloped H/L = 0.05 (e.g., Zilker and Hanratty 1979), where H is the wave height and L is the wavelength. The steepest laboratory waves cannot exist in nature, but their study is important for wind-wave

generation. Mature ocean surface waves tend to exhibit a very gentle slope in the deep ocean H/L ≈ 0.02-0.05. Beyond the threshold of 0.14 (Babanin *et al.* 2007) and 0.15 (Toffoli *et al.* 2010) for 2-D and 3-D progressive water waves, respectively, waves break and flow separation occurs. As waves approach the coast, they become increasingly nonlinear, and their study requires more representative wave models than the sinusoid models described in the studies above.

The present study examines aerodynamic drag on a rigid model of a shoaling wave surface in aerodynamic rough flow using the wind tunnel facility at Texas Tech University (TTU). To the author's knowledge, there are currently no laboratory experiments similar to this study, in which wind stress is determined over a nearshore wave train of this range. This paper does not attempt to address all the difficult and complicated issues associated with air-sea interaction. Rather, the motivation for this work is to provide some of the initial data to gain insight into nearshore wind stress by means of laboratory measurements over solid models, and to promote additional laboratory and observational research in this critical area.

2. Estimation of the drag coefficient

The horizontal component of the wind acting on the sea surface is called wind stress, and it arises from the vertical transfer of horizontal momentum. Wind stress over the ocean is formally defined as the retarding force per unit area exerted by the sea surface on the flow, and is typically described in terms of a 10 m surface drag coefficient C_D

$$\tau_w = \rho_a C_D \overline{U}_{10}^2 = \rho_a u_*^2 \tag{1}$$

Here, ρ_a is the density of air, u_* is the friction (or shear) velocity, and $\bar{U}_{10}$ (or $\bar{U}_r$) is the reference height mean wind speed measured at 10 m above mean sea level and averaged over the standard time period of 10 minutes. The drag coefficient can be thought of as a measure of sea surface roughness in the marine environment and is a function of at least fifteen properties and air-sea phenomena (Babanin and Makin 2008), the most common being sea state, atmospheric stability, and wind speed and direction (e.g., Donelan *et al.* 2004, Feddersen and Veron 2005).

The earliest estimates of momentum flux over the sea came from applying the profile method to a set of wind data. This method utilizes the logarithmic law, which is based on the flat-plate boundary layer theory of Prandtl and von Kármán. The log-law can be written as

$$\overline{U}(z) = \frac{u_*}{k} \ln\left(\frac{z-d}{z_o}\right) \tag{2}$$

where k is the von Kármán constant (determined experimentally to be k = 0.40 ± 0.01) and d is the displacement plane, which is typically taken to be at the MWL in the marine environment. The method of least squares is applied to the vertical mean wind speed profile to estimate u_* and z_o. It is based on the assumption that a nearly logarithmic mean wind velocity profile exists in the constant flux layer under neutral stability, horizontal homogeneity, and stationarity. This method is widely used in both field (e.g., Powell *et al.* 2003) and laboratory studies (e.g., Gong *et al.* 1999). Other techniques to estimate u_* include the eddy-correlation (e.g., Babanin and Makin 2008),

inertial dissipation (e.g., Pond *et al.* 1979), bulk aerodynamic (e.g., Yelland and Taylor 1996), turbulence intensity (e.g., Barthelmie *et al.* 1993), and gust factor methods (e.g., Wieringa 1993).

3. Shoaling wave model

Of critical importance to the validity of data collected in a laboratory setting is the model scale representation of the prototype. This is a relatively straight forward task for experiments utilizing rigid objects. However, in the present study, a level of complexity was added to this process by modeling a constantly evolving surface. In this case, an average or typical wave must be identified to generate a representative model.

Strong winds swirling around the low pressure centers of hurricanes impart a stress on the ocean surface. It is this transfer of momentum from the atmosphere to the ocean that generates wind waves. Hurricane waves are typically large in amplitude compared to oceanic waves that exist in mean conditions, and tend to vary considerably in both height and period. These defining characteristics of an ocean wave are primarily a function of wind speed and fetch length, and along with water depth, are the minimum set of parameters required to model an ocean wave.

Since there are nearly an infinite number of combinations of wave height and period, the wave shape to be studied was modeled after a typical hurricane-generated wave located near the coast. Based on an analysis of hurricane waves, a wave height of H = 5 m and period T = 12 s were selected as the prototype characteristics. For modeling purposes, water depth affects the relative location of this wave with respect to the coastline, and is the primary factor governing wave shape in the nearshore region. A water depth of h = 8 m was chosen, which places this wave in the shoaling region and seaward of the breaking waves in the surf zone. Although shoaling waves (and all nearshore waves) are inherently non-linear, a rough estimation of the wavelength L ≈ 100 m was determined using linear wave theory (e.g., Dean and Dalrymple 1991). The parameters H, h, and L (or T) provide the foundation for generating the model wave.

Using these parameters, a shoaling hurricane wave was created numerically by summing four wave harmonics:

$$\sum_{i=1}^{4} A_i \cos(ikx + \delta_i) \tag{3}$$

of differing amplitudes A, frequencies kx, and phases δ. The technique described in Eq. (3) generates a wave with a sharper crest and flatter trough, indicative of a shoaling wave. These types of waves are characterized by their asymmetry A_s and skewness S_k, which are a measure of the lack of symmetry with respect to the horizontal and vertical axes, respectively. Both A_i and δ_i were chosen by direct comparison with observed laboratory shoaling waves to yield the same skewness and asymmetry.

Statistically, a wave profile representative of the shoaling region was generated by matching S_k and A_s values to a numerical nonlinear wave study by Kennedy *et al.* (2000). Their results were in good agreement with the laboratory experiments by Mase and Kirby (1992) using irregular waves. Based on Fig. 10 in Kennedy *et al.* (2000), a range of values for asymmetry (0.10-0.30) and skewness (0.65-1.0) were identified to be matched by the model wave. After adjusting the harmonics, a representative shoaling wave shape was generated with asymmetry and skewness

values of 0.275 and 0.763, respectively. It should be emphasized that, by using this method, a statistically valid shoaling wave shape was generated for analysis in the wind tunnel.

A plot of the shoaling wave is shown in Fig. 1. For this nearshore wave to be oriented in an onshore wind flow regime, the gentle-sloped side of the wave faces out to sea and the steeper-sloped side towards the coast. This is typical for waves located near the coast (e.g., Dean and Dalrymple 1991). Onshore wind flow, left to right in Fig. 1, is the most critical flow direction for storm surge and for studying the boundary layer transition from the sea to the land. This is the wave orientation examined in this study.

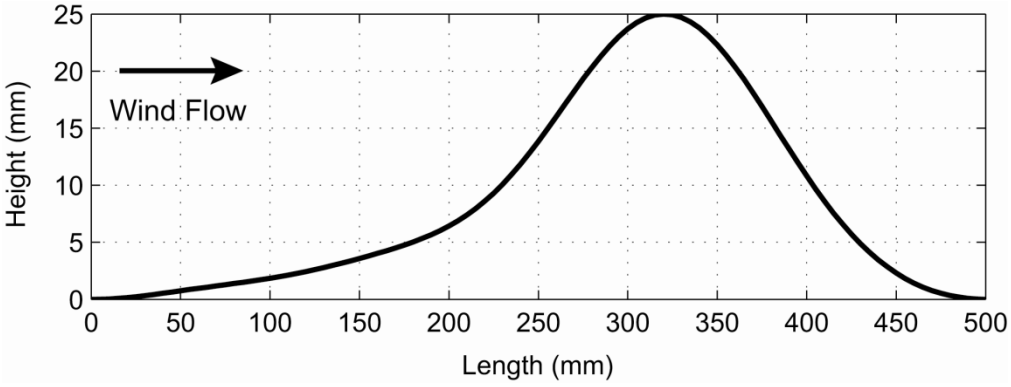

Fig. 1 Model scale dimensions of the shoaling wave

4. Experiment detail

4.1 Flow configuration

The TTU wind tunnel is powered by a single 250 hp axial flow fan, which is capable of generating empty tunnel wind speeds of 0-45 ms^{-1} in the boundary layer test section. The working section of the wind tunnel is 1.83 m wide by 1.25 m high and has a fetch length of 15.2 m spanning from the contraction outlet to the boundary layer test section. A detailed description of the TTU wind tunnel can be found in Zachry (2009). Based on the characteristics of the TTU wind tunnel compared to those of the shoaling wave model, a length scale of 1:200 was chosen for this study.

As for all wind tunnel experiments, the flow configuration and hence simulation of the atmospheric boundary layer is key to producing meaningful results. Here, the boundary layer was developed over a series of flow augmentation devices and wave models: 4 mm high shag carpet, an offshore wave train, and a shoaling wave train were placed along the wind tunnel fetch length. To generate initial turbulence and provide depth to the boundary layer, flow augmentation devices, in the form of a grid and fence barriers, were installed upstream. These devices were followed by a 3.2 m long strip of shag carpet on the flat wind tunnel surface. Next there was a series of six offshore wave models. They were covered by the carpet roughness and occupied 5 m of fetch. This roughness simulated deep water hurricane waves and provided a relatively natural transition of the boundary layer to the shoaling wave train under study.

Three variations of offshore wave shape were used to simulate air flow over deep water waves. The transition to shallow water was simulated by increasing the wave steepness *H/L* (with *H* remaining constant). The farthest upstream (i.e., offshore) wave was modeled after a deep water wave having the following characteristics: H = 5 m, T = 12 s, and L = 200 m (H/L = 0.025). The next set of model waves had wavelengths reduced to 170 m (H/L = 0.029), followed by a decrease to L = 130 m (H/L = 0.039). Due to the difficulty in constructing large sinusoid waves, triangular-shaped waves were used to simulate waves in deep water. Triangular waves shapes are considered acceptable since turbulent air flow over a triangle is similar to the flow over a sinusoid, and that the affects of the bluff body are far enough upwind as to have negligible impact on the flow over the shoaling wave models.

The shoaling wave train, consisting of eight waves and occupying a fetch length of 4 m, followed the offshore waves. They were constructed of ABS plastic using a 3-D printer. The models were precisely generated to the following characteristics: wavelength L = 500 mm, trough to crest wave height H = 25 mm, width W = 253 mm, and thickness D = 3.175 mm. They were oriented normal to the flow along the centerline of the wind tunnel. Since the wave models were relatively narrow compared to wind tunnel width ($W/W_{wt} = 0.14$), dummy shoaling wave models were placed on either side of the precise models to occupy nearly the remainder of the wind tunnel width. The dummy models were triangular in shape and had identical height and length dimensions, which ensured 2-D flow and prevented any spurious flow leakages.

The printing process resulted in an inherent roughness on the wave models. To characterize the roughness of the waves, a roughness Reynolds number was computed following Nikuradse (1933)

$$\mathrm{Re}_r = \frac{z_o u_*}{\nu_a} \tag{4}$$

where ν_a is the kinematic viscosity of air. Over the sea surface air flow is considered aerodynamically rough if $\mathrm{Re}_r > 2.0$ (e.g., Fairall *et al.* 1996, Zilitinkevich *et al.* 2001). A wavelength-averaged Re_r was computed by taking an arithmetic mean of the values obtained along the wave. The calculation showed that the flow was aerodynamically smooth with a roughness Reynolds number of 0.045. Aerodynamically rough flow was simulated by introducing upstream turbulence via placing square bass wood trips on the upstream models (e.g., Holmes 2007). The trips were 1.59 mm X 1.59 mm X 254 mm (HWL, 1/16 inch X 1/16 inch X 10 inch), oriented normal to the flow, and placed in approximately 20 mm increments along the arc of the waves (for a total of 25 trips on each wave). In addition to the turbulence trips upstream, local roughness was enhanced by placing a gridded fiberglass insect screen on the tested model. The grid size was 1.59 mm (1/16 inch). The roughness Reynolds number for this simulation was 3.1, indicative of aerodynamically rough flow with negligible dependence on Reynolds number.

When the developing boundary layer encounters the shoaling wave train, it adjusts to this underlying surface. Flow periodicity can be achieved since the underlying topography is periodic. Previous research has determined that if there are a sufficient number of waves, the flow is able to reach an equilibrium configuration (e.g., Beebe 1972). Counihan (1974) found that the flow essentially becomes periodic downstream of the third wave crest. Similarly, using a train of 16 steep laboratory waves, Gong *et al.* (1999) found that the flow reached a near-equilibrium, periodic state by the third or fourth waves. In the present study, measurements were taken over the sixth wave model with two waves following downstream, which prevents flow acceleration in

absence of the underlying surface roughness at the end of the wave train and allows the flow to reach a periodic state. Over a water wave surface, the transitional path length is much longer and on the order of tens of wavelengths (e.g., Soloviev and Kudryavtsev 2010), due to the fundamental turbulent-driven differences between turbulent air flow over a static and evolving fluid surface.

In order to relate wind tunnel measurements to full scale, length, velocity, and time scales were determined. As mentioned above, all models waves were scaled as 1:200. This scale reduction placed the standard 10 m meteorological reference height at 50 mm model scale (MS) above the displacement plane of 12.5 mm. For this experiment d was set at the theoretical mean water level of 0.5h = 12.5 mm. This displacement height essentially sets z = 0 at 12.5 mm. A velocity scale was chosen based on a wavelength-average of the five wind tunnel longitudinal (streamwise or U-component) reference height mean wind speeds $\bar{U}_r$ (described below). With an average value of 10.0 ms^{-1}, a velocity scale of 1:4 was selected. Full scale wind speeds of this magnitude will generate nearshore waves similar in height to the shoaling model utilized in this study. However, the actual wave heights observed in wind speeds of this magnitude will vary considerably and are highly dependent on the local bathymetry, fetch length, and many other factors (e.g., Dean and Dalrymple 1991).

4.2 Sampling methodology

Boundary layer profiles were measured using a Turbulent Flow Instrumentation (TFI) Cobra Probe sampling at a rate of 250 Hz. Wind and turbulence profiles, depicted in Fig. 2, were sampled at: location A at the leading edge of the sixth wave z_s = 0 mm (x/L = 0, where z_s is the height of the wave surface and x is the horizontal distance along the wave), location B on the upwind side of the wave at z_s = 12.5 mm (x/L = 0.482), location C directly above the wave crest z_s = 25 mm (x/L = 0.636), location D on the downwind side of the wave at z_s = 12.5 mm (x/L = 0.780), and location E at the end of the sixth wave z_s = 0 mm (x/L = 1.0).

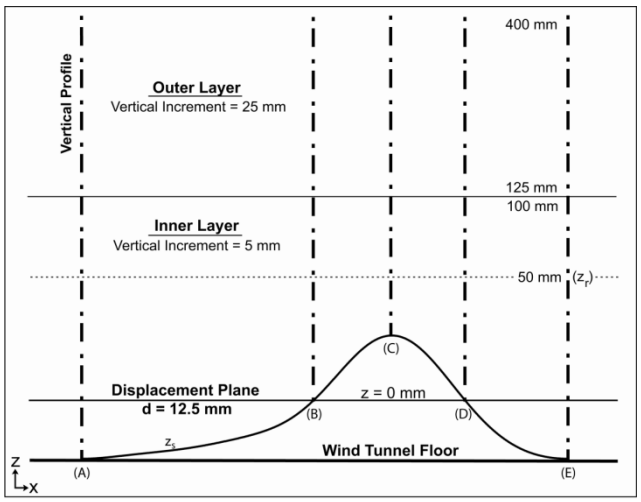

Fig. 2 Experimental plan for the vertical profiles sampled at five locations (A-E) along the wave

Profiles were divided into inner and outer layers. The inner layer was defined as the portion of wind profile below 100 mm and above *d*. Measurements within the inner layer were sampled in 5 mm vertical increments (1 m FS). Outer layer step size was increased to 25 mm (5 m FS), and reached a maximum height of 400 mm (80 m FS). A smaller step size was used in the inner layer to provide a detailed representation of the flow in this critical region. Since a displacement plane was employed, wind profiles began at different starting heights above the wave surface (either 2.5 or 5 mm) to keep uniform wind profile heights (relative to *d*) at each of the five locations. The profiles started at: 2.5 mm above z_s (10 mm below *d*) at locations A and E; 5 mm above z_s (5 mm above *d*) at locations B and D; 2.5 mm above z_s (15 mm above *d*) at location C. Measurements were taken below the displacement plane at locations A and E to obtain a complete wind profile, but these data were not used in the analysis. The sampling period at each step was 73.728 s, which represents just over an hour of prototype data. Regardless, wind data were stationary after about 40 s.

The sixth wave model was pressure tapped along its centerline. The taps were placed in 10 mm increments from the wave crest (x/L = 0.636) down both sides of the wave until reaching the half wave height (or amplitude *A*, z_s = 12.5 mm). Past the midway point (x/L = 0.482 on upwind portion and x/L = 0.780 downwind) taps were placed in 20 mm increments. Due to the wave asymmetry, the last upwind and downwind taps were located 14 mm and 7 mm from the end of the wave, respectively. A closer tap spacing was necessary near the crest to detect possible separated flow. The taps were labeled as 1-32, with tap number 1 being the farthest upstream. For the tap connections, a 90 mm length of vinyl tubing of 1.59 mm inner diameter (1/16 inch) X 3.18 mm outer diameter (1/8 inch) was secured to the wave model and connected to 2.38 mm inner diameter (3/32 inch) X 3.97 mm outer diameter (5/32 inch) tubing attached to the Scanivalve system. The total length of tubing for each tap was 290 mm. Pressure corrections were not necessary as this length provides good amplitude and phase characteristics (e.g., Holmes 2007).

The Scanivalve system was connected to a data acquisition computer scanning at 248 Hz (~5 Hz FS). Mean pressure coefficients C_p were computed using

$$\overline{C_{p_i}} = \overline{\left(\frac{\Delta p_i - p_{s_i}}{p_{dyn} - p_{s_i}} \right)} RHR \tag{5}$$

where Δp_i is the mean pressure difference between the local surface pressure and the static reference pressure measured at the pitot tube at tap *i*, p_{dyn} is the mean dynamic pressure at the pitot tube, and p_{si} is the mean static calibration pressure of the Scanivalve module. The pitot-static tube was located 0.95 m above the wind tunnel floor and 230 mm from the wall, which is well outside the local influence of the wave models. RHR is the reference height ratio correction determined by dividing the mean longitudinal velocity at the pitot tube by the mean longitudinal reference wind speed and squaring this value. With a mean reference height velocity of 10.0 ms^{-1} and mean free-stream velocity of 14.2 ms^{-1}, the RHR was 2.03. Time histories of C_p were tested for stationarity using the runs test and the reverse arrangement test (Bendat and Piersol 1986). The time series were stationary in both the first (mean) and second (variance) moments.

4.3 The simulated flow

Power spectral density functions (PSDs) were estimated to determine the quality of the simulated boundary layer compared to the marine environment. Time series of longitudinal wind speed taken at the reference height were broken into 10 min FS segments or windows (12 s MS). For each segment, power spectra were computed using Welch's averaged, modified periodogram method with 50% overlap of the neighboring data blocks and smoothed using a Hanning window (e.g., Bendat and Piersol 1986, Flandrin 1998). The presented PSDs are ensemble averages of the 11 individual PSDs generated for each time window and profile location. Reduced frequency $f_z = nz/\bar{U}_r$ (where n is the sampling frequency) and the normalized spectrum $nS_u(n)/u_*^2$ are plotted on the x- and y-axes, respectively in Fig. 3. Model scale wind spectra were compared with the offshore ocean based spectral model derived by Kareem (1985) at z_r

$$\frac{nS_U(n)}{u_*^2} = \frac{335 f_z}{(1+71 f_z)^{5/3}} \tag{6}$$

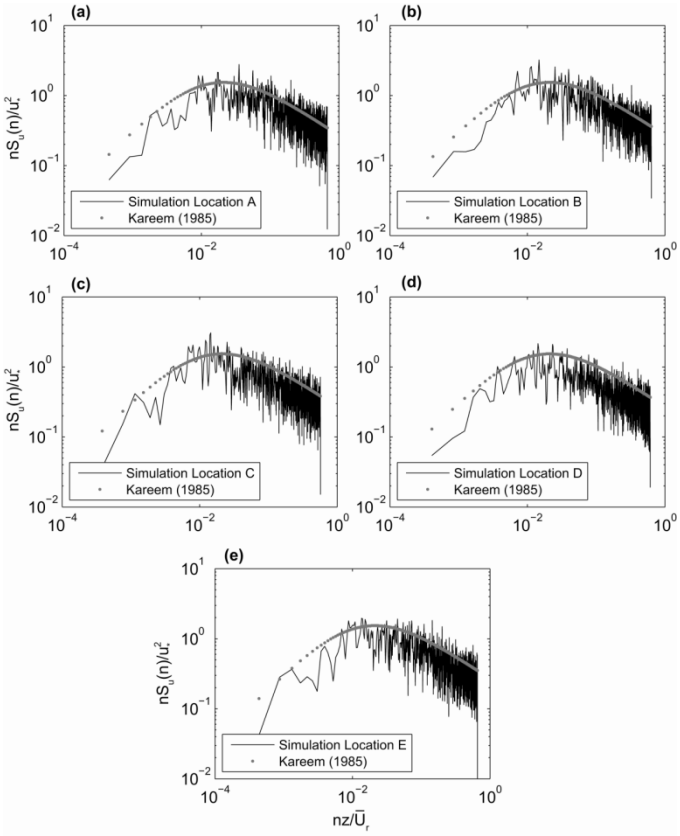

Fig. 3 Normalized power spectral density $nS_u(n)/u_*^2$ for the five profile locations A-E (a-e) compared with the offshore ocean based spectral model derived by Kareem (1985).

Results shown in Fig. 3 are in relatively good agreement with Eq. (6) at all profile locations. However, careful examination shows that the simulated wind spectra have less low frequency component, contain less high frequency energy, and have spectral peaks that align with the empirical relation. Slightly less low-frequency energy in the simulated spectra was to be expected due to the difficultly in reproducing low-frequency energy in wind tunnel simulations.

5. Results and discussion

5.1 Air flow over a shoaling wave train

Boundary layer profiles and surface pressure measurements were used to examine the air flow over a shoaling wave train. Plots of mean longitudinal wind speed $\bar{U}$, turbulence intensity I_u, and Reynolds shear stress $-\overline{u'w'}$ at each profile location are shown in Fig. 4. Exposures C and D in ASCE 7-05 (ASCE 2006), where applicable, are plotted for comparison. Height and wind speed are normalized by reference values, and shear stress is normalized by a wavelength-average of the shear velocity at the reference height.

Profile locations A and E are in the same wave-relative location. Excluding boundary layer growth, vertical profiles should, in theory, be nearly identical if the flow is in a near-equilibrium, approximately spatially periodic state. Fig. 4 shows that the addition of the turbulence trips upstream of the tested model introduced non-uniform upstream conditions. Flow over the smooth wave surface indicated equilibrium conditions (not shown). Addition of the turbulence trips caused slower wind speeds and significantly higher turbulence intensity and Reynolds shear stress in the lower levels at location A. These effects are observed throughout the profile, where wind speeds are slower than at location E, and shear stress and turbulence intensities are higher. Values differ most near the wave surface and decrease with increasing height. Below the reference height the largest percent differences between locations A and E at any vertical level are 4.8%, 10.7%, and 6.6% (2.6%, 5.7%, and 1.3% above z_r), respectively for $\bar{U}$, I_u, and $-\overline{u'w'}$. Some of this difference can be attributed to limitations of the Cobra probe. For $I_u < 30\%$ the probe is accurate to ± 0.5 ms^{-1}. Regardless, the flow is not in an equilibrium state at the tested model due to the turbulence trips upstream. The effect of this on the drag coefficient is discussed in the following section.

Wind speed profiles indicate that the flow remains attached over the wave surface and that there is a pronounced speed-up region over the wave crest. At location A, the wind profile corresponds closely with ASCE 7-05 Exposure C within the inner layer ($z/z_r \leq 2$), and wind speeds are lower than they are over the sloping portion of the wave. This result is due to the presence of a negative velocity perturbation, driven by the positive pressure gradient generated over the wave surface, which can extend well into the outer layer (e.g., Jackson and Hunt 1975). Negative velocity perturbations, and hence slower winds speeds result in higher turbulence intensities. At the upstream half wave height (location B), plots of I_u show decreased values near the wave surface in association with accelerated flow. This observation is consistent with surface pressure measurements, which indicate a strong negative pressure gradient (discussed below). Negative pressure perturbations drive positive velocity perturbations with height. Thus, wind speeds here are faster than at location A. At the wave crest (location C) there is pronounced region of accelerated flow. This phenomenon is similar to accelerated flow over a hill (e.g., Belcher and Hunt 1998). The speed-up region extends to about $z/z_r < 2.5$. This speed-up is consistent with a

significant decrease in turbulence intensity, in particular near the wave surface. At location D the lowest three measurement locations were taken near or below the wave height, and thus experience some wake-effects in the lowest levels. If the flow were to separate it would occur in lee of the crest. The wind profile shows no indication of separated flow, which was also confirmed by flow visualization. However, it is likely that the flow experienced intermittent separation (e.g., Donelan *et al.* 2006), but the mean flow remained attached. Mean pressure coefficients also show no indications of detached flow, but relatively high standard deviations exist in this region. At the final profile location, the mean flow continues to slow, and I_u continues to increase near the wave surface and throughout the inner layer.

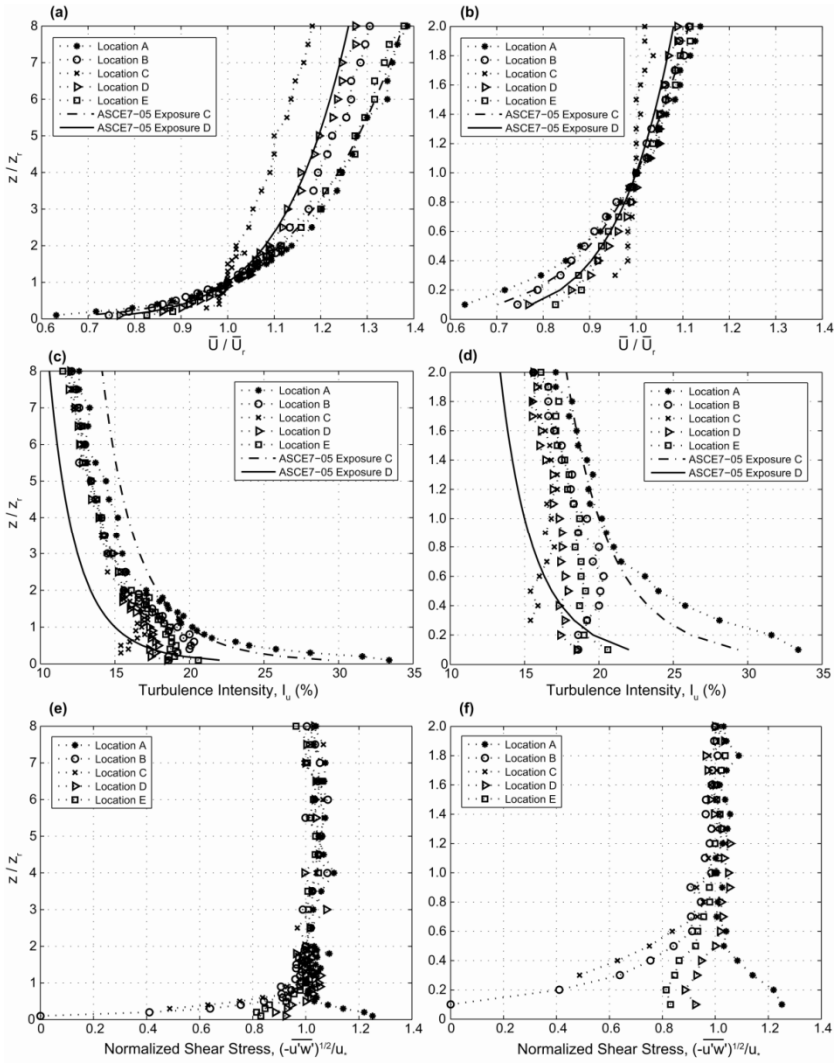

Fig. 4 Vertical profiles of mean longitudinal wind speed $\bar{U}$ (a,b), turbulence intensity I_u (c,d), and Reynolds shear stress $-\overline{u'w'}$ (e,f) for all profile locations (A-E) for the full (a,c,e) and inner boundary profiles (b,d,f)

Application of the profile method requires a constant flux of momentum with height to ensure validity of the Monin-Obukhov (MO) similarity theory, and more importantly the validity of the flow simulation. The MO theory is not valid below the surface layer in the interfacial sublayer. Within this sublayer, momentum flux increases from zero at the lower boundary and reaches a maximum value at its upper boundary. For this work, the boundary layer was not developed over a flat, homogeneous wind tunnel surface – wave height varies in the along-wind direction H = f(x). Hence, these roughness elements directly affect the wind speed and turbulence within the lower levels of the boundary layer. Plots of Reynolds shear stress (Fig. 4 (e) and (f)) indicate that it varies in the lowest levels, but is approximately constant at or slightly below the reference height. Only minimal departures in normalized shear stress profiles from 1.0 exist in the upper levels, and are likely due limitations in the flow measurement device.

Mean pressure coefficients, collected from 32 taps located along the centerline of the sixth wave model, are shown in Fig. 5. The shoaling wave shape is plotted on the bottom of the figure for convenience. This figure shows an average of the C_p values obtained at each tap for five independent scans (standard deviations of the average C_p were less than 0.008 at each tap) along with the mean ±1 standard deviation error bars. Non-equilibrium conditions are also evident in the pressure measurements, as the flow at the first few taps experience a slight deceleration compared to the last taps. In general, the pattern is asymmetric about the wave crest, which is driven by the asymmetric wave shape. As shown above in Fig. 4, a pronounced speed-up region is evident over the wave crest. On the wave surface, the speed-up region occurs after x/L = 0.417 (or tap #11), and accelerates rapidly until reaching a minimum pressure C_p = -0.672 at the crest. The flow decelerates smoothly in lee of the crest, indicative of attached flow. Flow visualization and wind measurements near the wave surface also confirmed that the mean flow remained attached. Pressure coefficients obtained at higher wind speeds (U_{10} > 15 ms^{-1}) were the same as those shown below, thus confirming Reynolds number independent flow within this range.

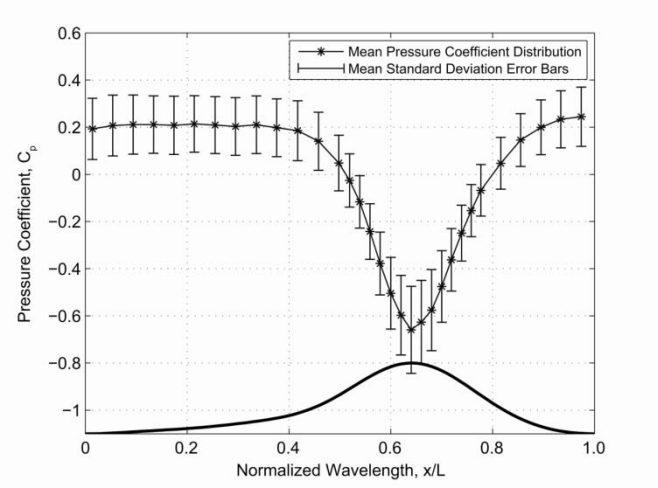

Fig. 5 Mean pressure coefficient distributions with ±1 standard deviation error bars derived from an average of five independent scans.

5.2 Drag coefficient analysis

The surface drag coefficient was estimated using the profile method applied to the inner layer wind speed profile. A characteristic wavelength-averaged value was obtained by computing an arithmetic mean of the C_D values obtained along the wave (see Table 1). Correlation coefficients were very good ($R^2 > 0.95$) for all locations, except over the crest where a pronounced speed-up region resulted in poor log-law fits.

It is known that the log-law is not valid in a region of accelerated flow over the wave crest. The speed-up region does not follow a logarithmic increase in wind speed with height and thus log-law fits become very poor. Use of the values obtained from a poor fit ultimately contaminates the results more significantly than omitting the region from the mean. The latter was chosen for this study, and thus location C was not included in the wavelength-average. In addition, since individual $\bar{U}$ measurements deviated from the log-law very near the model surface, profile method least square fits were modified by removing these data points from the regression. Poor agreement with the log-law near the wave surface was to be expected (e.g., Sjöblom and Smedman 2003). Including these values would introduce error into the u_* and z_o estimates. For example, if the lowest few wind speed data points were faster than that predicted by the log-law, smaller u_* and z_o values would result. In general, the profile method should not be employed in regions that deviate significantly from the log-law. All fits had the same maximum height of 100 mm, as chosen based on boundary layer growth over the shoaling waves. The height of 100 mm ensures that data employed in the fit are representative of the wave surface (topographically induced) and not the outer layer.

Table 1 Wind profile parameters and drag coefficient estimates

Profile Location	U_r (ms^{-1})	R^2	z_o (mm)	u_* (ms^{-1})	C_D (×1000)
A	9.23	0.998	0.183	0.663	5.17
B	9.88	0.993	0.097	0.632	4.09
C	11.0	—	—	—	—
D	10.2	0.978	5.63E-03	0.456	2.00
E	9.50	0.987	0.052	0.559	3.46
Mean	10.0	0.989	0.084	0.577	3.68
St. Dev.	0.690	0.008	0.075	0.092	1.30

Surface drag coefficients were relatively consistent along the wave. A minimum C_D was observed at location D. This location was likely affected by accelerated flow over the wave crest and some wake-effects in the lowest levels. This resulted in a less sheared profile, and thus smaller u_* and z_o values compared to the other wind profile locations. The drag coefficient was highest at location A, primarily due to the non-equilibrium conditions causing slower reference wind speeds

and higher shear velocity compared to location E. Although inclusion of this data point in the wavelength average yields a slightly high-biased value, it does not affect the overall results of the study (if the drag coefficient at location E is used as a replacement for location A, $C_D = 0.0033$). Other locations have higher $\bar{U}$ due to compressed streamlines over the wave crest and positive velocity perturbations over the sloped portion of the wave. However, locations A and E were located in a relatively flat portion of the wave, far enough away from the accelerated flow, as to not be significantly affected. Therefore, reference winds speeds were slower and drag coefficients were higher.

Table 2 Drag coefficient estimates over shoaling waves obtained for this study and the limited number full scale observations

Source	U_{10} (ms^{-1})	h (m)	H (m)	H/h	C_D (×1000)	Description
Present Study	40.0	8.00	5.00	0.625	3.68	Rough Surface
Anctil and Donelan (1996)	13.0	5.30	2.30	0.434	2.52	Lake Ontario
	14.1	5.20	1.62	0.312	2.84	Lake Ontario
	15.0	5.20	2.11	0.405	2.98	Lake Ontario
Vickery and Skerlj (2000)	24.0	47.5	Unknown	N/A	4.48	Hurricane Emily
	30.7	47.5	Unknown	N/A	6.13	Hurricane Emily
	20.1	13.0	Unknown	N/A	4.52	Hurricane Emily
	27.3	13.0	Unknown	N/A	7.02	Hurricane Emily
	29.9	13.0	Unknown	N/A	7.47	Hurricane Emily
Powell (2008)	20.3	< 50	Unknown	N/A	1.19	8 Hurricanes
	26.6	< 50	Unknown	N/A	1.85	9 Hurricanes
	33.0	< 50	Unknown	N/A	2.05	5 Hurricanes
	39.6	< 50	Unknown	N/A	3.22	5 Hurricanes

Drag coefficient values obtained herein and for the limited number of full scale observations over shoaling waves are provided in Table 2. Since the ocean surface is aerodynamically rough in winds greater than 8 ms^{-1}, the wind tunnel simulation is comparable to full scale measurements. A baseline study utilizing steep sinusoid waves was conducted by Zachry (2009) and the results are consistent with the deep water drag coefficients reported in Powell *et al.* (2003), where C_D values ranged from 0.0018 to 0.0027 for various scales of simulation. C_D values presented in Vickery and Skerlj (2000) are about 60% higher than the present study. Some of this difference can be attributed to their use of an indirect method to determine the drag coefficient, $C_D = [U_{10}^2/gz][U_{10}/c_p]$, where c_p is the wave phase speed and g is the gravitational constant.

Vickery and Skerlj (2000) did not provide wave heights, but they are likely large as the datasets used were sampled in hurricane conditions. The simulated shoaling wave drag coefficient is 32% higher than an average of the measurements obtained in Lake Ontario (Anctil and Donelan 1996). Wind speeds for their work are in the moderate regime, and wave heights are lower than those observed in hurricanes. Thus, it is not surprising that drag coefficients are lower than those measured in the present study. Recent measurements by Powell (2008) at depths less than 50 m in hurricanes show that C_D increases with wind speed over shoaling waves and reaches a maximum of 0.0032 for wind speeds of 39.6 ms^{-1}. This experiment estimates shoaling wave drag to be slightly (14%) higher. The wind tunnel results compare well to these limited studies, and thus provide some validation of the experiment design.

Form drag results from the interaction of air flow with objects immersed in a flow field and the eddying motions that result. Pressure drag is a primary function of the size and shape, hence 'form' of the object, and arises due to a combination of positive pressure on the upwind face and negative on the leeward. To examine the drag on the wave surface, a form drag coefficient C_{DF} was calculated by integrating the horizontal component of the mean surface pressure coefficients along the path length S using the following equation

$$C_{D_F} = \sum_{i=1}^{n} \frac{\delta S_i \overline{C_{p_i}} \cos(\alpha_i)}{\lambda} \tag{7}$$

where λ is the wavelength, δS_i is the distance between pressure taps, C_{pi} is the mean pressure coefficient at tap i, α_i is angle made between C_{pi} (normal to the wave surface) and the horizontal axis, and $cos(\alpha_i)$ gives the horizontal component or form drag. Following this equation, a form drag coefficient of 0.0055 was determined. This value represents the form drag on the wave surface as referenced to z_r.

The form drag values computed here are compared to sinusoidal waves in Fig. 6. Maximum wave slope for a sinusoid is easily computed as Ak, where A is the wave amplitude and k is the wave number. For progressive 2-D and 3-D water waves the critical wave slope is approximately 0.44 (Babanin *et al.* 2007) and 0.48 (Toffoli *et al.* 2010), respectively, after which waves break, flow separation occurs, and a near doubling of the drag is observed (e.g., Babanin *et al.* 2007). For an asymmetric wave, slopes differ on the upstream and downstream portions of the wave, and are 0.222 and 0.248, respectively, in the present study. The maximum upwind slope is used as the reference value in Fig. 6. Also, the RHR was removed from the computation of the form drag coefficient, as the comparison studies are normalized by the free-stream velocity (now C_{DF} = 0.0027). Results indicate that shoaling wave form drag is comparable to values over sinusoidal waves with slightly smaller maximum slopes. This result is in good agreement with Kuzan *et al.* (1989), who determined that flow separation occurs for a slope ≥ 0.3. Due to the flow remaining attached, shoaling wave form drag is considerably less than for sinusoidal waves with slopes of around 0.35-0.40, which are above the critical slope for separation. Beyond the threshold of 0.44 (represented by a solid vertical line in Fig. 6), the wave forms can no longer exist as natural water waves. The noticeable leveling off of the form drag coefficient for wave slopes exceeding 0.8, based on the C_{DF} value obtained by Beebe and Cermak (1972) for a wave slope of 1.27, is due to skimming flow (where a vortex resides between the wave crests and the flow above the wave does not penetrate into the troughs).

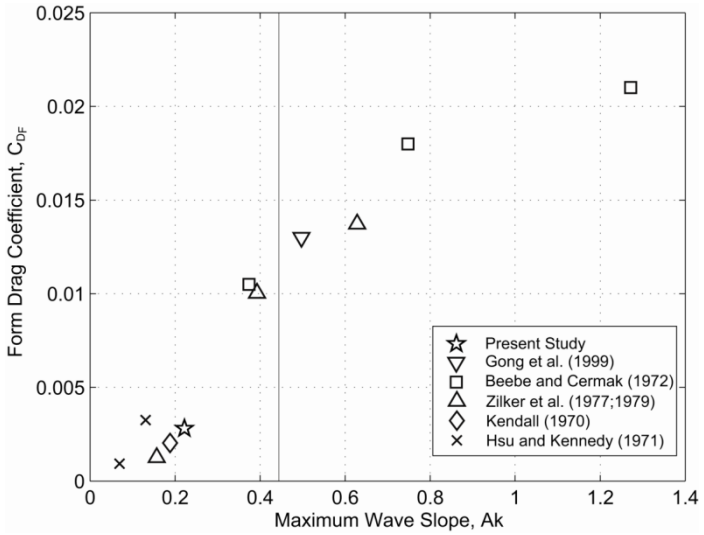

Fig. 6 Form drag coefficient for this study (asymmetric wave) and other laboratory studies that used sinusoidal wave shapes. The vertical line at Ak = 0.44 represents the critical slope for natural water waves

6. Conclusions

Since it is extremely difficult to obtain wind measurements over shoaling waves in large seas associated with hurricanes, laboratory measurements provide valuable insight. This study examined aerodynamically rough flow over a statically valid hurricane-generated shoaling wave train in simulated hurricane force winds (scaled 1:4) utilizing the wind tunnel at Texas Tech University. A 1:200 scale representation of a shoaling hurricane wave (with characteristics: depth h = 8 m, wave height H = 5 m, and wave period T = 12 s) was generated by summing four wave harmonics, and matching wave asymmetry and skewness values to those determined in Kennedy *et al.* (2000). Boundary layer profiles were sampled at five locations along the sixth wave in the train (with two waves downwind of the tested model) to determine the drag coefficient via the profile method. Results obtained in this study provide the following conclusions:

i. Wind tunnel simulation of air flow over a fixed wavy surface is not significantly different than that over actual water waves, and results provide valuable insight into the flow behavior. This statement is confirmed by the laboratory deep water baseline wave study conducted by Zachry (2009), in which results were consistent with the deep water values given by Powell *et al.* (2003). The shoaling wave drag coefficient computed in the laboratory compares well to the few observational studies. C_D estimates were 23% higher than those of Anctil and Donelan (1996) for winds of 15 ms^{-1} (H_s = 0.5 m), and 14% higher than Powell (2008) in hurricane conditions. This result suggests that wind tunnel simulations of this type likely offer an upper limit for wind stress compared to full scale.
ii. It was confirmed that wind stress over shoaling waves is higher than that over deep water waves. Powell *et al.* (2003) observed a maximum drag coefficient on the order of 0.0025 – the value obtained herein (0.0037) is approximately 50% higher. This result suggests that

depth-dependent parameterizations in storm surge models are needed, and that models using deep water parameterizations may be underestimating the wind setup contribution to surge generated in the shoaling wave region.

iii. Air flow over this shoaling wave train did not separate in lee of the crest. The flow remained attached and a pronounced speed-up region was present over the wave crest. If flow separation occurs in the field in strong winds, this study suggests that it is due to other phenomena (e.g., high frequency waves superimposed on low frequency waves, high winds shearing the crests of the waves, wave-wave interaction), and thus not steepness-induced separation. In the absence of flow separation, shoaling wave form drag is on the order of sinusoid waves with similar maximum slopes.

iv. Roughness lengths over shoaling waves are consistent with that of Exposure C in ASCE 7-05. The wavelength-averaged roughness length was 17 mm, with locally higher and lower values along the wave. This value is within the roughness category prescribed to structures located in hurricane prone regions. However, this work does not determine if the boundary layer that develops over shoaling waves is that experienced by structures located on the coast.

Acknowledgments

Funding support was provided by the National Science Foundation Integrative Graduate Education and Research Traineeship (IGERT) program under Grant No. 0221688 and Texas Tech University.

References

ASCE (2006), *Minimum design loads for buildings and other structures*, SEI/ASCE 7-05 (ASCE Standard No.7-05), American Society of Civil Engineers, Reston, VA.

Anctil, F. and Donelan, M.A. (1996), "Air-water momentum flux observations over shoaling waves", *J. Phys. Oceanogr.*, **26**(7), 1344-1353.

Babanin, A.V. and Makin, V.K. (2008), "Effects of wind trend and gustiness on the sea drag: Lake George study", *J. Geophys. Res.*, **113**(2), C02015.

Babanin, A.V., Chalikov, D., Young, I.R. and Savelyev, I. (2007), "Predicting the breaking onset of surface water waves", *Geophys. Res. Lett.*, **34**, L07605.

Babanin, A.V., Banner, M.L., Young, I.R. and Donelan, M.A. (2007), "Wave follower measurements of the wind input spectral function. Part 3. Parameterization of the wind input enhancement due to wave breaking", *J. Phys. Oceanogr.*, **37**, 2764-2775.

Banner, M.L. and Melville, W.K. (1976), "On the separation of air flow over water waves", *J. Fluid Mech.*, **77**(4), 825-842.

Barthelmie, R.J., Palutikof J.P., and Davies, T.D. (1993), "Estimation of sector roughness lengths and the effect on prediction of the vertical wind speed profile", *Bound.-Lay. Meteor.*, **66**(1-2), 19-47.

Beebe, P.S. and Cermak, J.E. (1972), *Turbulent flow over a wavy boundary*, Technical Report 16, CER71-72PSBJEC44, Fluid Dynamics and Diffusion Laboratory, Colorado State University, Fort Collins, CO.

Belcher, S.E. and Hunt, J.C.R. (1998), "Turbulent flow over hills and waves", *Annu. Rev. Fluid Mech.*, **30**, 507-538.

Bendat, J.S. and Piersol, A.G. (1986), *Random Data: Analysis and Measurement Procedures*, John Wiley & Sons, New York, NY.

Black, P.G., D'Asaro, E.A., Drennan, W.M., French, J.R., Niiler, P.P., Sanford, T.B., Terrill, E.J., Walsh, E.J., and Zhang, J.A. (2007), "Air-sea exchange in hurricanes: Synthesis of observations from the coupled boundary layer air-sea transfer experiment", *Bull. Amer. Meteor. Soc.*, **88**, 357-374.

Buckles, J.J., Hanratty, T.J., and Adrian, R.J. (1984), "Turbulent flow over large-amplitude wavy surfaces", *J. Fluid Mech.*, **140**, 27-44.

Charnock, H. (1955), "Wind stress on a water surface", *Q. J. Roy. Meteor. Soc.*, **81**, 639-640.

Counihan, J. (1974), "Flow over concatenated sinusoid hills", *Technical Report RD/L/N57/74*, Central Elec. Res. Lab., England.

Csanady, G.T. (2001), *Air-Sea Interaction: Laws and Mechanisms*. Cambridge University Press, New York, NY.

Dean, R.G. and Dalrymple, R.A. (1991), *Water wave mechanics for engineers and scientists*, World Scientific Press, Toh Tuck Link, Singapore.

Donelan, M.A., Haus, B.K., Ruel, N., Stianssnie, W.J., Graber, H.C., Brown, O.B. and Saltzman, E.S. (2004), "On the limiting aerodynamic roughness of the ocean in very strong winds", *Geophys. Res. Lett.*, **31**, L18306.

Fairall, C.W., Bradley, E.F., Rogers, D.P., Edson, J.B. and Young, G.S. (1996), "Bulk parameterization of air-sea fluxes in TOGA COARE", *J. Geophys. Res.*, **101**, 3747-3767.

Feddersen, F. and Veron, F. (2005), "Wind effects on shoaling wave shape", *J. Phys. Oceanogr.*, **35**, 1223-1228.

Flandrin, P. (1998), *Time-frequency/time-scale analysis*, Academic Press.

Gong, W., Taylor, P.A. and Dörnbrack, A.D. (1999), "Turbulent boundary-layer flow over fixed aerodynamically rough two-dimensional sinusoid waves", *J. Fluid Mech.*, **312**, 1-37.

Holmes, J.D. (2007), *Wind Loading of Structures*. 2nd edition, Taylor and Francis, London.

Hsu, H.T. and Kennedy, J.F. (1971), "Turbulent flow in wavy pipes", *J. Fluid Mech.*, **47**, 481-501.

Jackson, P.S. and Hunt, J.R. (1975), "Turbulent wind flow over a low hill", *Q. J. Roy. Meteor. Soc.*, **101**, 929-955.

Jarosz, E., Mitchell, D.A., Wang, D.W. and Teague, W.J. (2007), "Bottom-up determination of air-sea momentum exchange under a major tropical cyclone", *Science*, **315**(5819), 1707-1709.

Kareem, A. (1985), "Wind-induced response analysis of tension leg platforms", *J. Struct. Division - ASCE*, **111**(1), 37-55.

Kendall, J.M. (1970), "The turbulent boundary layer over a wall with progressive surface waves", *J. Fluid Mech.*, **41**(2), 259-281.

Kennedy, A.B., Chen, Q., Kirby, J.T. and Dalrymple, R.A. (2000), "Boussinesq modeling of wave transformation, breaking, and runup I: 1D", *J. Waterw. Port Coast. Ocean Eng.*, **126**(1), 39-47.

Kuzan, J.D., Hanratty, T.J. and Adrian, R.J. (1989), "Turbulent flows with incipient separation over solid waves", *Exps. Fluids*, **7**(2), 88-98.

Mase, H. and Kirby, J.T. (1992), "Hybrid frequency-domain KdV equation for random wave transformation", *Proceedings of the 23rd International Conference on Coastal Engineering*, New York, 474-487.

Nikuradse, J. (1933), "Laws of flow in rough pipes", *Technical report, NACA Technical Memo 1292*, National Advisory Commission for Aeronautics, Washington, DC.

Pond, S., Large, W.G., Miyake M. and Burling R.W. (1979), "A Gill twin propeller-vane anemometer for flux measurements during moderate and strong winds", *Bound.-Lay. Meteor.*, **16**, 351-364.

Powell, M.D. (2008), *High wind drag coefficient and sea surface roughness in shallow water*, Final Report to the Joint Hurricane Testbed.

Powell, M.D., Vickery P.J. and Reinhold, T.A. (2003), "Reduced drag coefficient for high wind speeds in tropical cyclones", *Nature*, **422**, 279-283.

Sjöblom, A. and Smedman, A. (2003), "Vertical structure in the marine atmospheric boundary layer and its implication for the inertial dissipation method", *Bound.-Lay. Meteor.*, **109**(1), 1-25.

Soloviev, Y.P. and Kudryavtsev, V.N. (2010), "Wind-speed undulations over swell: field experiment and interpretation", *Bound.-Lay. Meteor.*, **136**(3), 341-363.
Stanton, T.E., Marshall, D. and Houghton, R. (1932), "The growth of waves on water due to the action of the wind", *Proc. Roy. Soc.*, **137A**, 283-293.
Toffoli, A., Babanin, A., Onorato, M. and Waseda, T. (2010), "Maximum steepness of oceanic waves: field and laboratory experiments", *Geophys. Res. Lett.*, **37**(5), L05603.
Vickery, P.J. and Skerlj, P.F. (2000), "Elimination of exposure d along the hurricane coastline in ASCE 7", *J. Struct. Eng.- -ASCE*, **126**(4), 545-549.
Weaver, R.J. (2004), *Effect of wave forces on storm surge*. M.S. thesis, University of Florida, Gainesville, FL.
Westerink, J.J., Luettich, R.A., Feyen, J.C., Atkinson, J.H., Dawson, C.N., Roberts, H.J., Powell, M.D., Dunion, J.P., Kubatko, E.J. and Pourtaheri, H. (2008), "A basin to channel scale unstructured grid hurricane storm surge model applied to Southern Louisiana", *Mon. Weather. Rev.*, **136**(3), 833-864.
Wieringa, J. (1993), "Representative roughness parameters for homogeneous terrain", *Bound.-Lay. Meteor.*, **63**(4), 323-363.
Yelland, M.J. and Taylor, P.K. (1996), "Wind stress measurements from the open ocean", *J. Phys. Oceanogr.*, **26**, 541-558.
Zachry, B.C. (2009), *Wind-wave interaction in the nearshore environment*. Ph.D. thesis, Texas Tech University, Lubbock, TX.
Zilitinkevich, S.S., Grachev, A.A. and Fairall, C.W. (2001), "Scaling reasoning and field data on the sea surface roughness lengths for scalars", *J. Atmos. Sci.*, **58**, 320-325.
Zilker, D.P., Cook, G.W. and Hanratty, T.J. (1977), "Influence of the amplitude of a solid wavy wall on a turbulent flow", *J. Fluid Mech.*, **82**, 29-51.
Zilker, D.P. and Hanratty, T.J. (1979), "Influence of the amplitude of a solid wavy wall on a turbulent flow", *J. Fluid Mech.*, **90**, 257-271.